Available online at www.sciencedirect.com
SCIENCE DIRECT®
Mathematical Biosciences 200 (2006) 188–213
Mathematical Biosciences
www.elsevier.com/locate/mbs

A model for a G-protein-mediated mechanism for synaptic channel modulation

Gabriel Soto *, Hans G. Othmer

School of Mathematics, University of Minnesota, Minneapolis, MN 55455, United States

Received 23 May 2005; received in revised form 9 December 2005; accepted 13 January 2006
Available online 15 March 2006

Abstract

Neurons communicate with other neurons via specialized structures called synapses, at which the digital voltage signal encoded in an action potential is converted into an analog chemical signal. An action potential that arrives at the presynaptic face triggers release of neurotransmitter from vesicles in a calcium-dependent manner, and the neurotransmitter diffuses across the synaptic cleft and binds to receptors on the post-synaptic face, where it may trigger a postsynaptic action potential. Calcium is a critical component of the release process, and its spatio-temporal dynamics can control the release and can lead to facilitation or augmentation. However, how cells regulate cytoplasmic calcium so that exocytosis can be triggered successfully is still not completely understood. We propose a mechanism, based upon the experimental findings of Barrett and Rittenhouse [C.F. Barrett, A.R. Rittenhouse, Modulation of N-type calcium channel activity by G-proteins and protein kinase C, J. Gen. Physiol. 115 (3) (2000) 277], for the regulation of calcium influx through N-type channels in the presynaptic terminal by PKC and downstream effectors of G-protein activation. This proposed modulatory mechanism consists of a feedback loop involving cytoplasmic calcium, neurotransmitters and G-protein-coupled receptors. We study the dynamics of each component separately and then we address how kinetic properties of the components and the frequency of the stimuli affect the regulatory mechanisms presented here.

* Corresponding author. Present address: Center for BioDynamics, Boston University, 111 Cummington Street, Boston, MA 02115, United States. Tel.: +1 617 353 9543; fax: +1 617 353 4889.
E-mail address: gabys@math.bu.edu (G. Soto).

0025-5564/$ - see front matter © 2006 Elsevier Inc. All rights reserved.
doi:10.1016/j.mbs.2006.01.005

1. Introduction

At most synapses the increase in cytoplasmic calcium during synaptic transmission is due to the opening of voltage-gated calcium channels (VGCCs). The *calcium hypothesis* [2] postulates direct involvement of calcium in neurotransmitter release, and implies that regulatory mechanisms for intracellular calcium dynamics such as buffering [3] and calcium-induced-calcium release (CICR) [4] can play an important role in shaping the temporal profile of neurotransmitter release. However, the biophysical details as to how these processes affect neurotransmission are still not completely understood [5].

Regulation of calcium influx through VGCCs represents another mechanism by which cells control intracellular calcium dynamics during stimulation. There are many VGCCs present in the central nervous system (CNS), but N-type channels have been specifically linked to vesicle release [6]. Not only are N-type channel states modulated by the membrane potential [7] but they are also modulated by downstream effectors of G-proteins. For instance, Boland and Bean [8] found that the conductance of N-type channels in bullfrog sympathetic neurons was down-regulated by $\beta\gamma$ subunits. Swartz [9] showed that the conductance of N-type channels in rat central and peripheral neurons was up-regulated by protein kinase C (PKC), and found that phosphorylation of these channels by PKC prevents $\beta\gamma$-inhibition. Barrett and Rittenhouse [1] studied N-type calcium currents in sympathetic neurons and observed that such currents were modulated by both $\beta\gamma$ subunits and PKC simultaneously. They concluded that up- and down-regulation of the conductance are mutually exclusive i.e., whenever a $\beta\gamma$-subunit is bound to a channel site, the channel cannot be phosphorylated by PKC, and vice-versa. Moreover, they concluded that the only role of PKC phosphorylation is to prevent $\beta\gamma$-binding to the channel, thereby precluding inhibition without affecting channel conductance.

Autoreceptors, or G-protein-coupled receptors (GPCRs) are transmembrane receptor proteins located on the presynaptic plasma membrane which bind neurotransmitters released by the presynaptic neuron [10,11]. When occupied they activate intracellular G-proteins, which are also localized at the plasma membrane, by catalyzing the GDP-to-GTP exchange and the subsequent separation of the G-protein into its α and $\beta\gamma$ subunits. Autoreceptors have been linked to down-regulation of transmitter release [12], but there is also evidence that autoreceptors might be involved in vesicle release up-regulation [13]. The existence of autoreceptors and the fact that $\beta\gamma$ subunits and PKC are downstream effectors of G-protein activation suggests the existence of a membrane-delimited self-modulatory mechanism for vesicle release at the presynaptic face, as depicted in Fig. 1. First, VGCCs open and calcium levels increase, leading to vesicle localization at docking sites and neurotransmitter release. This produces a significant increase in the neurotransmitter concentration in the cleft and leads to increased occupancy of autoreceptors located on the presynaptic face, followed by increased G-protein activation. Downstream effectors of G-protein activation, such as $\beta\gamma$ subunits and activated PKC, then modify the conductances of VGCCs. Our objective in this paper is to develop and analyze a theoretical model for such a modulatory mechanism, using experimental results on the modulation of N-type channels.

Bertram and Behan [14] developed a simplified scheme for inhibition of N-type channels based on the work of Boland and Bean [8], who studied an eight-state model for a single N-type channel. Their model incorporates equations for the membrane potential and channel inhibition, but does

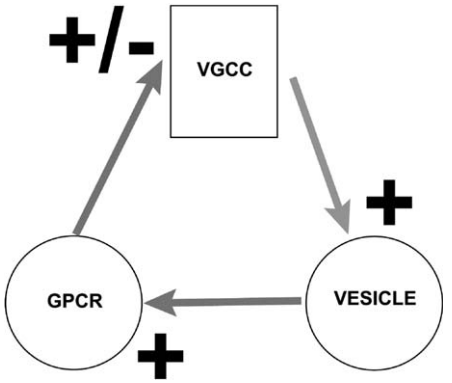

Fig. 1. A schematic representation of the postulated modulation of VGCCs on the presynaptic face. Upon stimulation, VGCCs open and the intracellular calcium concentration rises near the membrane. This causes calcium sensors on vesicles to trigger exocytosis (the + sign signifies that calcium activates vesicle fusion with sites on the plasma membrane). This leads to the release of neurotransmitters into the extracellular space and an increase in the occupancy of autoreceptors. Binding triggers two different biochemical pathways, one of which increases the conductance of VGCCs, and the other which decreases it.

not include the dynamics of G-protein activation and subsequent channel inhibition, nor the effect of PKC on relieving this inhibition. Here we develop a simplified version of the kinetic scheme in [8] in which we assume that channels can be in one of three distinct states of modulation: bare, inhibited or phosphorylated. Each of these can be open or closed, and in addition there is an intermediate non-conducting state. We incorporate the dynamics of PKC activation and binding to the channel, of neurotransmitter binding to autoreceptors, and of G-protein activation, in contrast with the model in [14] , which assumes that neurotransmitter binding is at equilibrium and which does not consider G-protein dynamics. We include all the reaction steps in these subprocesses, which are assumed to follow mass-action kinetics, because this enables us to follow the response on all time scales relevant to synaptic transmission. Even though the dimensionality of the resulting model is quite large, it is possible to identify different time scales for the processes involved in the modulation of N-type channels by G-protein activation and to use singular perturbation to reduce the dimensionality.

Both up- and down-regulation of calcium-influx through N-type VGCCs by G-protein activation are slow processes compared to fast synaptic transmission (cf. Section 3). Hence, such modulations would also depend, for instance, on the frequency of the stimuli and the kinetic properties of autoreceptors. In Section 5 we present numerical simulations showing how both modulatory pathways depend on frequency and autoreceptor kinetic properties.

2. The processes in the model

In Fig. 2 we show a schematic of all the components in the model and the interactions amongst them. Because numerous processes are incorporated in the model, we first give a chronological description of the major steps before giving the details of the individual steps:

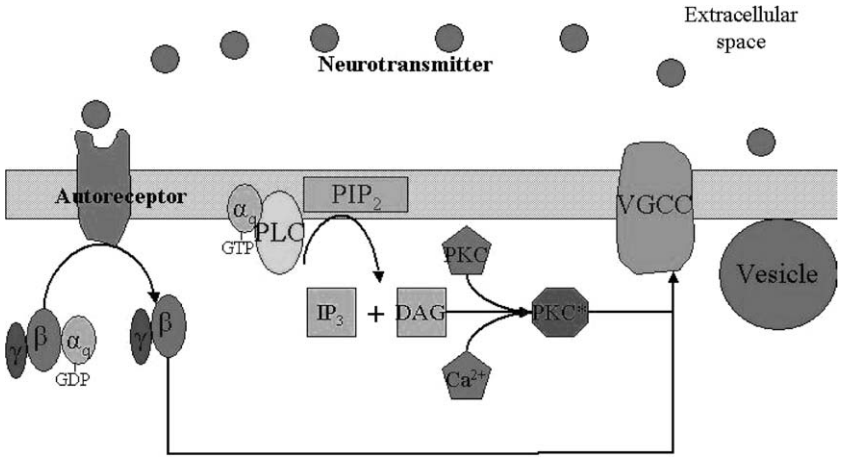

Fig. 2. A schematic description of the localization of the components of the model.

1. an action potential opens VGCCs on the presynaptic face;
2. intracellular calcium increases near the presynaptic face and binds to vesicles;
3. vesicle fusion and neurotransmitter release occur;
4. calcium also binds to inactive PKC;
5. neurotransmitter binds to autoreceptors, thereby activating G-proteins;
6. the $\beta\gamma$ subunits bind to VGCCs and the α subunits activate PLC;
7. PLC–PIP_2 generates DAG and IP_3;
8. generation of DAG-PKC-Ca (PKC^a), the active form of PKC;
9. PKC^* phosphorylates VGCCs.

The number of parameters needed to describe all of the steps involved in these events is quite large, but a non-dimensional analysis done later yields the following hierarchy of time scales and the events that occur on each of the scales.

- *fast time scale* (T):
  - opening and closing of VGCCs
  - vesicle release
- *intermediate time scale* (hydrolysis of GTP):
  - neurotransmitter binds to autoreceptors
  - activation of PLC
  - binding of Ca to PKC
- *slow time scale* (G-protein activation):
  - activation of G-proteins to produce the activated G_α^a and the $G_{\beta\gamma}$ subunits
  - activation of PKC to produce PKC^a.

We shall assume that VGCCs and GPCRs are co-localized and uniformly distributed in the presynaptic membrane Γ_c, and that vesicles are uniformly distributed in the presynaptic part of

a strip around Γ_c that we call the *active zone* (Fig. 3). Calcium and vesicle dynamics are defined on the presynaptic side of the active zone and the interaction between neurotransmitter and GPCRs occurs in the synaptic cleft.

We assume that each of the N-type calcium channels involved in synaptic transmission can be in one of the seven states shown in Fig. 4. The vertical transitions are modulated by membrane potential, with kinetic rates as in [14]. The horizontal transitions are modulated by downstream effectors of G-protein and PKC activation discussed earlier. The symbols and nomenclature for the channel states correspond to those in [1]. The governing equations for these steps and those in the remaining subcomponents are given in the following section.

We also assume that there is a pool of vesicles of fixed size in the presynaptic terminal and a finite number of uniformly-distributed release sites on the membrane to which vesicles bind in a calcium-dependent manner. Fig. 5 shows the kinetic scheme used for vesicle release. Similar schemes, in which the number of vesicle states varies from 3 to 5, have been used when studying transmitter release [15], but changes in the number of vesicle states do not modify the qualitative dynamics of vesicle release. B_i represents the fraction of vesicles with 0, 1, 2, 3 or 4 calcium ions bound and E corresponds to the release sites after vesicle fusion. The rate γ at which vesicles fuse

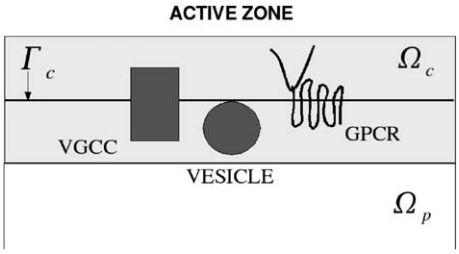

Fig. 3. A schematic description of the active zone, which comprises two narrow strips on both sides of Γ_c. The width of the active zone on both sides of Γ_c is $\mathcal{O}(10)$ nm. In particular, the extracellular side of the active zone corresponds to the entire synaptic cleft, since its width is $\mathcal{O}(10)$ nm.

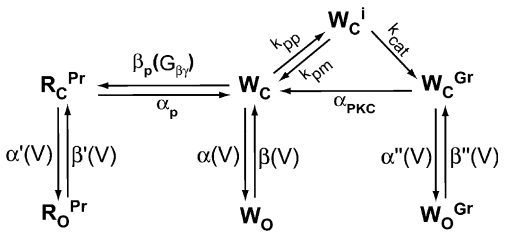

Fig. 4. The kinetic scheme for the state transitions of N-type channels. The different states are defined as follows: R^{Pr} corresponds to the inhibited state *resistant to phosphorylation* by PKC, W represents the willing state of the channel and W^{Gr} is the phosphorylated state that is *resistant to inhibition* by $\beta\gamma$ subunits. Subscripts c, o represent the closed and open states, respectively, and the vertical transitions that are voltage dependent. Superscripts Pr denote a phosphorylation-resistant state, while superscripts Gr denote an inhibition-resistant state. The nomenclature inhibited and willing is from [1]. Note that the transition rate from W_c to R_c^{Pr} depends on the concentration of $\beta\gamma$-subunits.

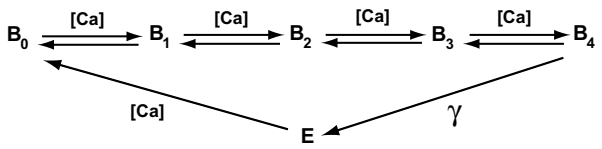

Fig. 5. Kinetic representation of vesicle release, adapted from [15]. The replenishment of vesicles from the vesicle pool is assumed calcium-dependent as in [18,17].

with the membrane and release neurotransmitter is related to the intrinsic probability p that a docked vesicle releases neurotransmitter under some reference conditions (e.g., a long interval of no stimuli followed by a single action potential) in some complicated and as yet unknown manner, since it accounts for many factors. The precise relationship used in the computations will be given later. Thomson [16] pointed out the important role that p plays in neurotransmission, since synapses with a low release probability may show *facilitation* (an increase in vesicle release under repeated stimulation) and those with a high release probability can show depression (reduction of vesicle release under repeated stimulation).[1] We also assume that the replenishment of empty sites is calcium-dependent, as was suggested earlier [17,18].

The activation of G-proteins occurs via a kinetic mechanism adapted from [19].

$$N + R \underset{k_{m1}}{\overset{k_{p1}}{\rightleftarrows}} NR \tag{1}$$

$$NR + G \underset{k_{m2}}{\overset{k_{p2}}{\rightleftarrows}} NRG \tag{2}$$

$$NRG \overset{k_{\text{act}}}{\rightarrow} NR + G_{\alpha}^{\text{a}} + G_{\beta\gamma} \tag{3}$$

$$G_{\alpha}^{\text{a}} \overset{k_{\text{hyd}}}{\rightarrow} G_{\alpha}^{i} + P_i \tag{4}$$

$$G_{\alpha}^{i} + G_{\beta\gamma} \overset{k_6}{\rightarrow} G \tag{5}$$

Here N, R and NR are the concentrations of neurotransmitter, and bare and bound autoreceptors, respectively, G is the concentration of G-protein on the presynaptic face, NRG is the concentration of the complex of ligand, receptor and G-protein; G_{α}^{a} and $G_{\beta\gamma}$ are the concentrations of the activated α subunits and the $\beta\gamma$ subunits, respectively, and G_{α}^{i} is G_{α}-GDP, i.e., the inactive form of G_{α}. The parameter values used here are chosen from those used in [19–21], and are given in Table 3.

Finally, the scheme for the activation of PKC, which includes generation of DAG by cleavage of PIP_2 by activated phospholipase C (PLC), is adapted from [22–24].

[1] The term facilitation has been used to characterize two different processes, one related to vesicle release and the other to the effect of depolarizations on $\beta\gamma$-subunit inhibition of N-type channels. Here we use the same term to refer to both processes, and which is referred to is clear from the context.

$$\mathrm{PLC}^i + G_\alpha^{\mathrm{a}} \underset{k_{1b}}{\overset{k_{1f}}{\rightleftarrows}} \mathrm{PLC}^{\mathrm{a}} \tag{6}$$

$$\mathrm{PLC}^{\mathrm{a}} + \mathrm{PIP}_2 \underset{k_{2b}}{\overset{k_{2f}}{\rightleftarrows}} \mathrm{PLC}^* \overset{k_a}{\rightarrow} \mathrm{DAG} + \mathrm{IP}_3 + \mathrm{PLC}^{\mathrm{a}} \tag{7}$$

$$\mathrm{PKC}^i + \mathrm{Ca} \underset{k_{7b}}{\overset{k_{7f}}{\rightleftarrows}} \mathrm{PKC}^* \tag{8}$$

$$\mathrm{PKC}^* + \mathrm{DAG} \underset{k_{8b}}{\overset{k_{8f}}{\rightleftarrows}} \mathrm{PKC}^{\mathrm{a}} \tag{9}$$

Here PLC^i and $\mathrm{PLC}^{\mathrm{a}}$ are the inactive and active forms of phospholipase C, $\mathrm{PLC}^* = \mathrm{PLC}^{\mathrm{a}} - \mathrm{PIP}_2$ is a complex; PIP_2 is a hydrophobic lipid on the plasma membrane; DAG is diacylglycerol; and PKC^i, PKC^* and $\mathrm{PKC}^{\mathrm{a}}$ are the inactive, intermediate and active forms of protein kinase C, respectively.

3. The governing equations and the parameter values

In this section we present the full system of governing equations for the model in dimensional form. This system has the general structure

$$\begin{aligned} &\frac{\mathrm{d}\mathbf{x}}{\mathrm{d}t} = \mathbf{H}(\mathbf{x}), \\ &\mathbf{x}(0) = \mathbf{x}_0, \end{aligned} \tag{10}$$

where $\mathbf{x} = (x_1, \ldots, x_n)$, x_i represents the 'density' of the ith species, n is the number of species and x_0 represents the initial value of the state. Because the number of species involved is large, we present the system of equations in modular form, corresponding to GPCR activation, channel modulation, vesicle release, and finally, to PKC activation. The different sub-processes in the model have been studied elsewhere, and to the extent possible we have tried to keep the same notation and units used in these studies. Some parameters are given in volumetric concentrations, others in surface-density units, and throughout we use $\theta_p = 100\ \mu\mathrm{m}^{-1}$ when necessary, as the conversion factor between surface and volume units.

3.1. Channel dynamics

The seven equations governing the channel dynamics are as follows:

$$\frac{\mathrm{d}[R_{\mathrm{c}}^{\mathrm{Pr}}]}{\mathrm{d}t} = \beta_p[W_{\mathrm{c}}][G_{\beta\gamma}] + \beta'(V)[R_{\mathrm{o}}^{\mathrm{Pr}}] - (\alpha_p + \alpha'(V))[R_{\mathrm{c}}^{\mathrm{Pr}}], \tag{11}$$

$$\frac{\mathrm{d}[R_{\mathrm{o}}^{\mathrm{Pr}}]}{\mathrm{d}t} = \alpha'(V)[R_{\mathrm{c}}^{\mathrm{Pr}}] - \beta'(V)[R_{\mathrm{o}}^{\mathrm{Pr}}], \tag{12}$$

$$\frac{\mathrm{d}[W_{\mathrm{c}}]}{\mathrm{d}t} = \alpha_p[R_{\mathrm{c}}^{\mathrm{Pr}}] + \beta(V)[W_{\mathrm{o}}] + \alpha_{\mathrm{pkc}}[W_{\mathrm{c}}^{\mathrm{Gr}}] - (\beta_p[G_{\beta\gamma}] + \alpha(V) + k_{pp}[\mathrm{PKC}]^{\mathrm{a}})[W_{\mathrm{c}}] + k_{pm}[W_{\mathrm{c}}^i], \tag{13}$$

Table 1
Parameter values for the channel dynamics: $\beta\gamma$ inhibition from [8,32]; PKC-phosphorylation from, [37,38]; channel density from [7]

Symbol	Value
C_t	3.3×10^{-4} μmol m^{-2}
α_p	0.25 s^{-1}
β_p	0.1 μM^{-1} s^{-1}
k_{pp}	0.1 μM^{-1} s^{-1}
k_{pm}	1 s^{-1}
α_{pkc}	0.25 s^{-1}
k_{cat}	10 s^{-1}

$$\frac{d[W_o]}{dt} = \alpha(V)[W_c] - \beta(V)[W_o], \tag{14}$$

$$\frac{d[W_c^{Gr}]}{dt} = k_{cat}[W_c^i] + \beta''(V)[W_o^{Gr}] - (\alpha_{pkc} + \alpha''(V))[W_c^{Gr}], \tag{15}$$

$$\frac{d[W_c^i]}{dt} = k_{pp}[PKC^a][W_c] - (k_{pm} + k_{cat})[W_c^i], \tag{16}$$

$$\frac{d[W_o^{Gr}]}{dt} = \alpha''(V)[W_c^{Gr}] - \beta''(V)[W_o^{Gr}]. \tag{17}$$

Here $[R_c^{Pr}]$, $[R_o^{Pr}]$ are the inhibited closed and open states, $[W_c^{Gr}]$, $[W_o^{Gr}]$ are the phosphorylated closed and open states and $[W_c]$, $[W_o]$ are the closed and open states. $[W_c^i]$ is the intermediate state before phosphorylation. The superscript Pr means that the channel is PKC-phosphorylation resistant; the superscript Gr means that the channel is G-protein-inhibition resistant (this nomenclature is from [1]). Note that $[R_c^{Pr}] + [R_o^{Pr}] + [W_c^i] + [W_c^{Gr}] + [W_o^{Gr}] + [W_c] + [W_o] = C_t$, where C_t is the channel density given in Table 1.

In this scheme the transmembrane voltage V modulates the opening and closing rates. The specific dependence on V is given by $\alpha(V) = 900\exp(V/22)$ s^{-1}, $\beta(V) = 30\exp(-V/14)$ s^{-1}, $\alpha' = \alpha/8$ and $\beta' = 8\beta$ as in [8]. In addition, $\alpha'' = \alpha$ and $\beta'' = \beta$, since Barrett and Rittenhouse [1] concluded that the effect of phosphorylation on N-type channels is to prevent inhibition, rather than to affect channel conductance.

3.2. Vesicle equations

The equations for the vesicle states shown in Fig. 5 are as follows:

$$\frac{d[E]}{dt} = \gamma[B_4] - k^+[Ca][E], \tag{18}$$

$$\frac{d[B_0]}{dt} = k^+[Ca][E] + k_{off}[B_1] - 4k_{on}[Ca][B_0], \tag{19}$$

$$\frac{d[B_1]}{dt} = 4k_{on}[Ca][B_0] + 2k_{off}[B_2] - (k_{off} + 3k_{on}[Ca])[B_1], \tag{20}$$

Table 2
Parameter values for the vesicle scheme in Fig. 5 from [15,17]

Symbol	Value
k^+	1 $\mu M^{-1}\,s^{-1}$
k^-	0 s^{-1}
k_{on}	97 $\mu M^{-1}\,s^{-1}$
k_{off}	9500 s^{-1}
p	0.01
nrs	30

$$\frac{d[B_2]}{dt} = 3k_{on}[Ca][B_1] + 3k_{off}[B_3] - (2k_{off} + 2k_{on}[Ca])[B_2], \tag{21}$$

$$\frac{d[B_3]}{dt} = 2k_{on}[Ca][B_2] + 4k_{off}[B_4] - (3k_{off} + k_{on}[Ca])[B_3], \tag{22}$$

$$\frac{d[B_4]}{dt} = k_{on}[Ca][B_3] - (\gamma + 4k_{off})[B_4]. \tag{23}$$

Here $[B_0]+[B_1]+[B_2]+[B_3]+[B_4]+[E] = nrs$, where nrs is the number of release sites on the presynaptic terminal. It is assumed that a single vesicle contains 3000–5000 transmitter molecules (quantal content) and that the diffusion coefficient of neurotransmitters is $\mathcal{O}(700)\ \mu m^2\,s^{-1}$ [25]. Table 2 shows the set of parameter values used for vesicle release here.

The parameter γ in (23) measures the rate at which vesicles with four calcium ions bound fuse and release their neurotransmitter. If the intrinsic release probability p is low, γ should be small, whereas for high release probability, γ should be large. Hence, we simply postulate that $\gamma = 4k_{off}p/(1-p)$, and this γ has the desired properties. Moreover, for $p = 0.5$, it follows that $\gamma = 4k_{off}$, which indicates that there is no preference for a given vesicle with four calcium ions bound to either fuse with the membrane or to release one calcium ion. Even though there is no direct experimental evidence for the expression chosen, it is appropriate for limiting forms of p. This assumption implies that the mean time vesicles spend in the four-calcium bound state (B_4) is $(1-p)/(4k_{off})$, and for fixed p, the larger k_{off} is, the harder it is to release a vesicle, i.e., the release of calcium from the release machinery is the dominant process. If we fix k_{off}, the assumption is consistent with physiological data for $p \sim 0$ and for $p \sim 1$.

3.3. G-protein activation

The equations for the G-protein activation steps are as follows:

$$\frac{d[R]}{dt} = -k_{p1}[N][R] + k_{m1}[NR], \tag{24}$$

$$\frac{d[NR]}{dt} = k_{p1}[N][R] + (k_{m2} + k_{act})[NRG] - (k_{p2}[G] + k_{m1})[NR], \tag{25}$$

$$\frac{d[G]}{dt} = k_6[G_{\beta\gamma}][G^i_\alpha] + k_{m2}[NRG] - k_{p2}[NR][G], \tag{26}$$

Table 3
Parameter for activation of G-protein from [19–21]

Symbol	Value
k_{p1}	50 $\mu M^{-1}\ s^{-1}$
k_{m1}	5 s^{-1}
k_{p2}	$10^3\ m^2\ \mu mol^{-1}\ s^{-1}$
k_{m2}	0 s^{-1}
k_{act}	1.8 s^{-1}
k_{hyd}	27 s^{-1}
k_6	$10^5\ m^2\ \mu mol^{-1}\ s^{-1}$
R_t	$1.67 \times 10^{-3}\ \mu mol\ m^{-2}$
G_t	$1.67 \times 10^{-3}\ \mu mol/m^{-2}$

$$\frac{d[NRG]}{dt} = k_{p2}[NR][G] - (k_{act} + k_{m2})[NRG], \tag{27}$$

$$\frac{d[G_\alpha]}{dt} = k_{act}[NRG] + k_{1b}[PLC^a] - (k_{hyd} + k_{1f}[PLC^i])[G_\alpha], \tag{28}$$

$$\frac{d[G_{\beta\gamma}]}{dt} = k_{act}[NRG] + \alpha_p[R_c^{Pr}] - (k_6[G_\alpha^i] - \beta_p[W_c])[G_{\beta\gamma}], \tag{29}$$

$$\frac{d[G_\alpha^i]}{dt} = k_{hyd}[G_\alpha] - k_6[G_{\beta\gamma}][G_\alpha^i]. \tag{30}$$

We also have the conservation laws $[R] + [NR] + [NRG] = R_t$, $[G] + [NRG] + [G_\alpha] + [G_\alpha^i] + [PLC^a] + [PLC^*] = G_t$ and $[G] + [NRG] + [G_{\beta\gamma}] + [W_c] + [R_c^{Pr}] = G_t$, where R_t and G_t are the total autoreceptor and G-protein density on the presynaptic face. $[PLC^*]$ is the concentration of inactive PLC and $[R_c^{Pr}]$ is the concentration of channels in the inhibited state (cf. Table 3). The parameter values are as in [19], except for the G-protein activation rate k_{act} and ATP-hydrolysis rate k_{hyd}, which are at least one order of magnitude higher than in [19] (the values used here are taken from [21]).

3.4. PLC activation and PKC generation

$$\frac{d[PLC^i]}{dt} = -k_{1f}[G_\alpha^a][PLC^i] + k_{1b}[PLC^a], \tag{31}$$

$$\frac{d[PLC^a]}{dt} = k_{1f}[G_\alpha^a][PLC^i] + k_{1b}[PLC^a] - k_{2f}[PIP_2][PLC^a] + (k_{2b} + k_a)[PLC^*], \tag{32}$$

$$\frac{d[PLC^*]}{dt} = k_{2f}[PIP_2][PLC^a] + (k_{2b} + k_a)[PLC^*], \tag{33}$$

$$\frac{d[DAG]}{dt} = k_a[PLC^*] - k_{deg}[DAG] - k_{8f}[PKC^*][DAG] - k_{8b}[PKC^a], \tag{34}$$

$$\frac{d[PKC^i]}{dt} = -k_{7f}[PKC^i][Ca] + k_{7b}[PKC^*], \tag{35}$$

Table 4
Parameter values for activation of PKC: PLC dynamics from [23], DAG dynamics from [22] and PKC dynamics from [24]

Symbol	Value
$[PLC]_0$	1.2×10^{-4} μmol/m^{-2}
$[PLC]_0$	0–100 μM
$[PIP_2]$	0.1 μmol/m^{-2}
k_{1f}	1.1×10^6 m^2 μmol^{-1} s^{-1}
k_{1b}	1 s^{-1}
k_{2f}	2.14×10^5 m^2 μmol^{-1} s^{-1}
k_{2b}	5.25 s^{-1}
k_a	5–10 s^{-1}
k_{deg}	2–5 s^{-1}
k_{7f}	5 μM^{-1} s^{-1}
k_{7b}	50 s^{-1}
k_{8f}	1.5×10^4 μM^{-1} s^{-1}
k_{8b}	0.15 s^{-1}

We have used $\theta_p = 100\ \mu m^{-1}$ (Γ_c surface area to active zone volume) to convert concentrations (μM) into surface densities (μmol m^{-2}).

$$\frac{d[PKC^*]}{dt} = -k_{7f}[PKC^i][Ca] - k_{7b}[PKC^*] - k_{8f}[PKC^*][DAG] + k_{8b}[PKC^a], \tag{36}$$

$$\frac{d[PKC^a]}{dt} = k_{8f}[PKC^*][DAG] - k_{8b}[PKC^a]. \tag{37}$$

Both PLC and PKC are conserved and therefore $[PLC^i] + [PLC^a] + [PLC^*] = [PLC]_0$ and $[PKC^i] + [PKC^*] + [PKC^a] = [PKC]_0$, where $[PLC]_0$ is the total PLC density on the presynaptic face and $[PKC]_0$ is the total PKC concentration in the active zone. Parameter values for these equations are given in Table 4.

3.5. Neurotransmitter in the cleft

$$\frac{d[N]}{dt} = \gamma \tilde{V}[B_4] - t_{[N]}[N], \tag{38}$$

where $\tilde{V}$ depends on the total number of release sites and the number of transmitter molecules contained in each vesicle. Since the cleft has a width of 10–20 nm and we assume that the release sites are uniformly distributed on Γ_c, it takes $\mathcal{O}(10^{-6})$ s for a molecule to reach the post-synaptic membrane (using a diffusion coefficient for neurotransmitters of 700 μm^2/s, cf. Table 2). Hence, we may assume that the concentration of neurotransmitters in the cleft is spatially uniform. The decay rate of neurotransmitters in the cleft is then given by $t_{[N]} = \mathcal{O}(10/\mu s)$, values for neurotransmitter decay from [26].

3.6. Intracellular calcium

Calcium concentrations as high as 100 μM are needed to trigger exocytosis at fast synapses [27], and we use this fact to estimate space and time scales for neurotransmitter release. Syntaxin

(a membrane protein of the SNARE complex necessary for vesicle fusion) has been found to be functional only when co-expressed with N-type calcium channels [28]. This suggests that we can assume both the release machinery and VGCCs to be co-localized in the active zone, and this was the basis for choosing the thickness of the active zone to be $\mathcal{O}(10)$ nm. If we assume that calcium enters into the cytoplasm through a point source corresponding to a single channel, and ignore boundary effects, we estimate that the time needed to reach 100 μM for distances $\mathcal{O}(10\,\text{nm})$ is $T = \mathcal{O}(0.1)$ ms, which we choose as a characteristic time scale for vesicle release. On this time scale the relevant calcium concentration is that in a microdomain surrounding a release site. We assume that in the intracellular active zone underlying the presynaptic face, the calcium concentration evolves according to

$$\frac{\mathrm{d}[\mathrm{Ca}]}{\mathrm{d}t} = \Lambda([W_{\mathrm{O}}] + [R_{\mathrm{O}}^{\mathrm{Pr}}] + [W_{\mathrm{O}}^{\mathrm{Gr}}]) - k_{[\mathrm{Ca}]}[\mathrm{Ca}], \tag{39}$$

where $\Lambda = 10^6 C_{\mathrm{t}} N_{\mathrm{a}} \delta \theta_p$, where N_{a} is Avogadro's number and $\delta = 5.12 \times 10^{-12}\,\mu\text{mol}\,\text{s}^{-1}$, which represents the calcium current through a single channel [29], and [Ca] is measured in μM. We approximate the calcium efflux from this active region into the bulk cytoplasm by the term $k_{[\mathrm{Ca}]}[\mathrm{Ca}]$, where $K_{[\mathrm{Ca}]}^{-1} = \mathcal{O}(10\,\mu\text{s})$ is the time constant for this process.

Note that we have neglected other possible regulatory mechanisms such as buffering. The rationale behind this assumption is the following: numerical simulations suggest that on space and time scales given by L and T, respectively, both the *excess buffer approximation and the pure diffusion approximation* [29] are good estimates for the effect of slow buffers such as EGTA on calcium profiles, whereas the *rapid buffer approximation* only holds for space scales at least two orders of magnitude higher than the one assumed here [30]. This assumption leads to an upper bound for the dynamics of calcium during synaptic transmission, which for slow buffers is a good approximation. The effect of buffering and other calcium-regulatory mechanisms such as CICR, are outside the scope of this work and deserve a careful analysis, which we defer to another paper.

4. Analysis of the model

We shall analyze the dynamics of VGCC-modulation, vesicle release and GPCR-activation separately to determine characteristic time scales for each process, and then compare these time scales to a characteristic time scale for vesicle release, which we choose to be $T = \mathcal{O}(0.1)$ ms, based on the delay between channel opening and beginning of transmitter release [27]. In the sequel, we shall call the *active phase* the time during which the channels are open, and the *passive phase* the time during which the channels are closed.

4.1. Channel dynamics

The dynamics of N-type channels during the passive phase (slow time scale) is governed by

$$\frac{\mathrm{d}[R_{\mathrm{c}}^{\mathrm{Pr}}]}{\mathrm{d}t} = \beta_p[W_{\mathrm{c}}][G_{\beta\gamma}] - (\alpha_p)[R_{\mathrm{c}}^{\mathrm{Pr}}], \tag{40}$$

$$\frac{\mathrm{d}[W_{\mathrm{c}}]}{\mathrm{d}t} = \alpha_p[R_{\mathrm{c}}^{\mathrm{Pr}}] + \alpha_{\mathrm{pkc}}[W_{\mathrm{c}}^{\mathrm{Gr}}] + k_{pm}[W_{\mathrm{c}}^{i}] - (\beta_p[G_{\beta\gamma}] + k_{pp}[\mathrm{PKC}^{\mathrm{a}}])[W_{\mathrm{c}}], \tag{41}$$

$$\frac{d[W_c^i]}{dt} = k_{pp}[PKC^a][W_c] - (k_{pm} + k_{cat})[W_c^i], \tag{42}$$

$$\frac{d[W_c^{Gr}]}{dt} = k_{cat}[W_c^i] - \alpha_{pkc}[W_c^{Gr}]. \tag{43}$$

We may suppose that $[R_c^{Pr}] + [W_c] + [W_c^{Gr}] + [W_c^i] = C_t$, since to lowest order during the passive phase $[R_o^{Pr}] = [W_o] = [W_o^{Gr}] = 0$. Let us define $R = [R_c^{Pr}]/C_t, W = [W_c]/C_t, P^i = [W_c^i]/C_t$ and $P = [W_c^{Gr}]/C_t$, which represent the fractions of channels in the inhibited, willing, intermediate (bound to PKC), and phosphorylated closed state, respectively. If we take $\tau = \alpha_p t$, where $\alpha_p^{-1} \gg T$ is the $\beta\gamma$-subunit release rate (cf. Table 1), then the non-dimensionalized set of equations for the reduced channel dynamics (corresponding to (40)–(43)), is given by

$$\begin{aligned}
\frac{dR}{d\tau} &= gW - R,\\
\frac{dW}{d\tau} &= R + P - gW - \tilde{\eta}W + P^i,\\
\frac{dP^i}{d\tau} &= \tilde{\eta}W - (1+\eta)P^i,\\
\frac{dP}{d\tau} &= \eta P^i - P,
\end{aligned} \tag{44}$$

where $g = [G_{\beta\gamma}]/K_{\beta\gamma}$ and $K_{\beta\gamma}$ is the dissociation constant for a $\beta\gamma$-subunit from an N-type channel. Note that we have taken $\alpha_{pkc} = \alpha_p$ and $k_{pm}/\alpha_p = \mathcal{O}(1)$. Then $\tilde{\eta} = [PKC^a]/K_{PKC}$ where $K_{PKC} \propto k_{pm}/k_{pp}$. Finally, $\eta = k_{cat}/\alpha_{pkc}$.

The steady state values for R and P obtained from Eq. (44) are given by

$$\begin{cases} R = \dfrac{g}{(1+g) + \mathrm{pkc}(1+\eta)}, \\ P = \dfrac{\eta\,\mathrm{pkc}}{(1+g) + \mathrm{pkc}(1+\eta)}, \end{cases}$$

where $\mathrm{pkc} = [PKC^a]/K_m$ and K_m is the Michaelis–Menten constant for PKC. The steady-state fraction of channels in the inhibited and phosphorylated states depend on g and pkc. Moreover, the size of η determines the strength of the competition between the two modulatory pathways at steady state. In fact

$$\frac{R}{P} = \frac{1}{\eta}\frac{g}{\mathrm{pkc}}$$

gives an estimate, for fixed values of g and pkc, as to whether inhibition or phosphorylation is the dominant modulation of VGCCs. For the parameter values chosen, $\eta = \mathcal{O}(50)$, which implies that small increases in PKC levels would lead to a large increase in the steady levels of phosphorylated channels. In other words, the rate at which the channel is dephosphorylated determines the levels of activated PKC necessary to overcome $\beta\gamma$-subunit inhibition.

4.2. Vesicle dynamics

There are two distinct time scales, which are determined by the levels of calcium during the active and passive phases, that are important for analyzing the vesicle dynamics. Both can be

estimated by $(k_{on}[Ca])^{-1}$, which is the mean time between binding of successive calcium ions to sites on a vesicle. During the passive or resting phase between widely-spaced stimuli the intracellular calcium concentration is $[Ca] = \mathcal{O}(0.1)$ μM, and $k_{on}[Ca] = \mathcal{O}(k_{act})$, which is comparable the time scale for G-protein activation (cf. Tables 2 and 3). In the active phase calcium is 1000-fold higher ($[Ca] = \mathcal{O}(100)$ μM) and $k_{on}[Ca] = \mathcal{O}(T^{-1})$. Thus the second scale is comparable to the vesicle release time estimated earlier from the time required for calcium to rise sufficiently.

If we define $y_{19} = E/nrs$, $y_{20} = B_0/nrs$, $y_{21} = B_1/nrs$, $y_{22} = B_2/nrs$, $y_{23} = B_3/nrs$ and $y_{24} = B_4/nrs$, where *nrs* is the number of release sites, then the vesicle dynamics can represented as

$$\dot{X} = AX, \tag{45}$$

where $X = (y_{19}, y_{20}, y_{21}, y_{22}, y_{23}, y_{24})$ and

$$A = (a_{ij}) = \begin{cases} a_{11} = -a_{21} = -\epsilon_3, & \\ a_{ii} = i - 6 + (i-2)\epsilon_1 & 2 \leqslant i \leqslant 5, \\ a_{i-1i} = (i-2)\epsilon_1 & 2 \leqslant i \leqslant 6, \\ a_{i+1i} = 6 - i & 2 \leqslant i \leqslant 5, \\ a_{16} = 4\epsilon_1\epsilon_2, & \\ a_{66} = -4\epsilon_1(1+\epsilon_2), & \\ a_{ij} = 0 & \text{otherwise.} \end{cases}$$

Here $\epsilon_i = K_D/[Ca]$, $\epsilon_2 = p/(1-p)$ and $\epsilon_3 = k^+/k_{on}$, $K_D = k_{off}/k_{on}$.

The first case is when $k_{on}[Ca] = \mathcal{O}(k_{act})$, which corresponds to $\epsilon_1 \gg 1$. In this case, Eq. (45) can be approximated to lowest order by

$$\frac{dy_{19}}{d\tau} = -\epsilon_3 y_{19}$$

and

$$y_{21} = y_{22} = y_{23} = y_{24} = 0.$$

This implies that the rate of convergence to $X = (0,1,0,0,0,0)$ ($B_0 \to nrs$) depends, to lowest order on ϵ_3 i.e., the rate at which the empty sites are replenished.

The second case obtains when $k_{on}[Ca] = \mathcal{O}(T^{-1})$, i.e., $\epsilon_1 = \mathcal{O}(1)$. We set $\epsilon_1 = 1$, and then the steady fraction of vesicles with four calcium ions bound is given by

$$\frac{3}{4}\frac{\epsilon_3}{12\epsilon_3 + 3\epsilon_2 + 16\epsilon_2\epsilon_3}.$$

If $\epsilon_2 \ll 1$ i.e., the release probability p is small, the steady fraction of vesicles ready to release is approximately $1/16 = 0.0625$. Note that the steady level of B_4 is independent of p, which is an indication that for small p, the synapse may show facilitation. For $\epsilon_2 \gg 1$ i.e., large release probability, it follows that to lowest order, $y_{24} = 0$. The steady fraction of empty sites y_{19} is approximately

$$\frac{3}{3 + 16\epsilon_3},$$

which gives an estimate of the number of vesicles released. In particular, when $\epsilon_3 \ll 1$ (slow replenishment of vesicles at the active zone), all vesicles attached to the membrane at the active zone are released and hence repeated stimulation would lead to synaptic depression [16].

The analysis shows that both the release probability and the replenishment rate determine the dynamics of release sites during the active and passive phase. The rate of replenishment determines how fast the release machinery recovers from the state $y_{20} \sim 1$ between spikes. With the parameter values chosen for this scheme, it follows that for small release probability, about 6% of the total number of vesicles will be available for release. This suggests that synapses with low release probability can sustain vesicle release without depleting the vesicle pool provided the frequency of stimulation is greater than or equal to k^+[Ca]. For high release probability ($\epsilon_2 \gg 1$), the fraction of empty sites only depends on ϵ_3. This suggests that high-frequency stimuli (frequencies greater than k^+[Ca]) would lead to synaptic depression.

4.3. G-protein activation

The time constant for G-protein activation, k_{act}^{-1}, can be regarded as a characteristic time scale for the activation of the modulatory pathways for the VGCCs. Next we analyze the dynamics of G-protein activation on this time scale, which is $\mathcal{O}(1)$ s, and thus much slower than the time scale for vesicle release.

Let us define $\tau = k_{\text{act}}t$, $y_5 = [R]/R_{\text{t}}$, $y_6 = [NR]/R_{\text{t}}$, $y_8 = [NRG]/R_{\text{t}}$ where R_{t} represents the density of autoreceptors on the membrane (in μmol/m^2), and $y_7 = [G]/G_{\text{t}}$, $y_9 = [G_\alpha]/G_{\text{t}}$, $y_{10} = [G_{\beta\gamma}]/G_{\text{t}}$ and $y_{11} = [G_\alpha^i]/G_{\text{t}}$ where G_{t} is the density of G-protein (cf. Table 3.) The corresponding non-dimensional system of equations for G-protein activation is given by

$$\begin{cases} \dfrac{dy_5}{d\tau} = v\left(-\dfrac{[N]}{K_{\text{aut}}}y_5 + y_6\right), \\ \dfrac{dy_6}{d\tau} = v\left(\dfrac{[N]}{K_{\text{aut}}}y_5 - y_6\right) + y_8 - \dfrac{k_{p2}G_{\text{t}}}{k_{\text{act}}}y_6y_7, \\ \dfrac{dy_7}{d\tau} = \dfrac{k_6G_{\text{t}}}{k_{\text{act}}}y_{10}y_{11} - \dfrac{k_{p2}G_{\text{t}}}{k_{\text{act}}}y_6y_7, \\ \dfrac{dy_8}{d\tau} = \dfrac{k_{p2}G_{\text{t}}}{k_{\text{act}}}y_6y_7 - y_8, \\ \dfrac{dy_9}{d\tau} = y_8 + \dfrac{k_{1b}[\text{PLC}]_0}{k_{\text{act}}G_{\text{t}}}y_{28} - \left(\dfrac{k_{\text{hyd}}}{k_{\text{act}}} + \dfrac{k_{1f}[\text{PLC}]_0}{k_{\text{act}}}y_{27}\right)y_9, \\ \dfrac{dy_{10}}{d\tau} = y_8 + \dfrac{\alpha_pR_{\text{t}}}{k_{\text{act}}G_{\text{t}}}R - \left(\dfrac{k_6G_{\text{t}}}{k_{\text{act}}}y_{11} + \dfrac{\beta_bR_{\text{t}}}{k_{\text{act}}}W\right)y_{10}, \\ \dfrac{dy_{11}}{d\tau} = \dfrac{k_{\text{hyd}}}{k_{\text{act}}}y_9 - \dfrac{k_6G_{\text{t}}}{k_{\text{act}}}y_{10}y_{11}, \end{cases} \tag{46}$$

where R and W are as in Section 4.1, and $y_{27} = [\text{PLC}^i]/[\text{PLC}]_0$ and $y_{28} = [\text{PLC}^a]/[\text{PLC}]_0$. From the parameter values given in Tables 1, 3 and 4, we have that $k_{\text{hyd}}/k_{\text{act}} \gg 1$, $k_6G_{\text{t}}/k_{\text{act}} \gg 1$, $k_{1b}[\text{PLC}]_0/(k_{\text{act}}G_{\text{t}}) \gg 1$, $\alpha_pR_{\text{t}}/(k_{\text{act}}G_{\text{t}}) \ll 1$, $\beta_bR_{\text{t}}/(k_{\text{act}}) \ll 1$ and $k_{1f}[\text{PLC}]_0/k_{\text{act}} \ll 1$. Here $[N]$ is the concentration of neurotransmitter in the cleft, and $K_{\text{aut}} = k_{m1}/k_{p1}$ is the affinity of the receptor (since

$k_{p2}G_t/k_{act} = \mathcal{O}(1)$, we set it equal to 1). The conservation laws are $y_5 + y_6 + y_8 = 1$, $y_7 + y_8 + y_9 + y_{11} + [PLC]_0/G_t y_{27} + [PLC]_0/G_t y_{28} = 1$ and $y_7 + y_8 + y_{10} + y_{11} + C_t/G_t R + C_t/G_t W = 1$. Therefore, to lowest order we have that the receptor-GPCR, subsystem decouples from the rest of the system obtaining

$$\begin{cases} \dfrac{dy_5}{d\tau} = \nu\left(-\dfrac{[N]}{K_{aut}}y_5 + y_6\right), \\ \dfrac{dy_6}{d\tau} = \nu\left(\dfrac{[N]}{K_{aut}}y_5 - y_6\right) + y_8 - y_6 y_7, \\ \dfrac{dy_7}{d\tau} = -y_6 y_7, \\ \dfrac{dy_8}{d\tau} = y_6 y_7 - y_8, \\ y_9 = y_{10} y_{11} = 0. \end{cases} \tag{47}$$

Note that since $C_t/G_t = [PLC]_0/G_t = \mathcal{O}(10^{-1})$, we may assume that the conservation laws for the reduced system (47) are $y_5 + y_6 + y_8 = 1$, $y_7 + y_8 + y_9 + y_{11} = 1$ and $y_7 + y_8 + y_{10} + y_{11} = 1$.

The ratio $\nu = k_{m1}/k_{act}$ of the release rate of neurotransmitter from the autoreceptor to the G-protein activation rate will determine how the interaction between neurotransmitters and autoreceptors affects VGCC-modulation. The first case is $\nu \gg 1$, and in this case we have that $y_5 = K_{aut}/[N]y_6$ to lowest order in the small parameter ν^{-1}, i.e., neurotransmitter binding equilibrates rapidly. We can then further reduce (47) to

$$\begin{cases} \dfrac{dy_6}{d\tau} = y_8 - y_6 y_7, \\ \dfrac{dy_7}{d\tau} = -y_6 y_7, \\ \dfrac{dy_8}{d\tau} = y_6 y_7 - y_8. \end{cases} \tag{48}$$

We recall that $y_5 + y_6 + y_8 = 1$ and $y_7 + y_8 + y_{10} + y_{11} = 1$, and then use the conservation conditions to obtain

$$\begin{cases} \dfrac{dy_6}{d\tau} = 1 - \dfrac{[N] + K_{aut}}{[N]}y_6 - y_6 y_7, \\ \dfrac{dy_7}{d\tau} = -y_7 y_6. \end{cases} \tag{49}$$

From the first of these equations it follows that significant G-protein activation, which requires occupied receptors, will occur on the time scale k_{cat}^{-1} only if $K_{aut} = [N]$. Under physiological conditions, neurotransmitter release during an action potential is terminated rapidly [31], and neurotransmitter clearance from the cleft occurs on a time scale $\mathcal{O}(1)$ ms [26]. Thus, on the time scale k_{cat}^{-1} for activation of G-proteins, $N \ll 1$, which implies that unless $K_{aut} \ll 1$ (i.e., high affinity receptors), G-protein activation will be negligible.

The second case is $\nu = \mathcal{O}(1)$. In this situation, it is possible to estimate a range of frequencies for which saturation effects would render the VGCC-modulation independent of the stimulation

frequency. Frequencies that would cause an increase in neurotransmitter concentration such that $[N] \gg K_{\text{aut}}$ on the time scale $\mathcal{O}(k_{\text{act}}^{-1})$, would yield $y_6 \sim 1$ (Eq. (47)) and the modulation of VGCCs would become tonic.

4.4. PLC and PKC activation

PKC activation depends on both DAG and intracellular calcium. DAG-generation occurs on a time scale $\mathcal{O}(k_{\text{hyd}}^{-1})$, corresponding to GTP-hydrolysis, and this is faster that G-protein activation and hence $\beta\gamma$ inhibition. Therefore significant increases in intracellular calcium concentrations on $\mathcal{O}(k_{\text{hyd}}^{-1})$ would elicit significant levels of activated PKC. Thus, depending on the regulatory mechanisms of intracellular calcium such as buffering or CICR, it is possible for VGCC up-regulation by PKC to prevail over $\beta\gamma$ inhibition [30].

5. Simulations of the model

From the analysis in the preceding section we conclude that modulation of VGCCs by G-protein activation occurs on a slower time scale than the time scale relevant for synaptic transmission. This suggests that we should investigate how such modulation is affected by repeated stimulation, since a single spike would not produce any significant increase in the levels of inhibited or phosphorylated channels. First we present simulations of the full model with a stimulation protocol similar to that in [1, Fig. 1, p. 279]. Then we address the dependence of the maximal fraction of inhibited and phosphorylated channels on stimulation frequency and the kinetic properties of autoreceptors.

Fig. 6 shows simulations of the full model, using the stimulation protocol depicted in part A of Fig. 6, for different values of the total concentration of PKC, $[\text{PKC}]_0$. For low concentrations of PKC ($[\text{PKC}]_0 = 1\ \mu\text{M}$), more than 50% of the channels are inhibited after one 10 mV step, which leads to an approximately 45% reduction in the calcium concentration (cf. Fig. 7). This is in agreement with the percentage reduction in currents through N-type channels observed experimentally [1]. If we increase the concentration of PKC to $[\text{PKC}]_0 = 10\ \mu\text{M}$, the peak fraction of inhibited channels after the second 10 mV depolarization step is about the same as in the previous case, and there is approximately a 5% decrease in the fraction of inhibited channels after the third 10 mV depolarization compared to the case for $[\text{PKC}]_0 = 1\ \mu\text{M}$. (cf. left panel Fig. 6). When $[\text{PKC}]_0$ is very high (100 μM), there is a significant decrease in the fraction of inhibited channels compared to $[\text{PKC}]_0 = 1$ after the second 10 mV step depolarization (about 10% reduction), and a 40% reduction after the third 10 mV step. This is due to the fact that as we increase $[\text{PKC}]_0$, there is a corresponding increase in the fraction of phosphorylated channels (cf. right panel in Fig. 6). Note that after the first depolarization step, the rate of increase in the inhibited channel fraction is the same for all PKC levels (cf. Fig. 6). This is an indication of the fact that ($\beta\gamma$-subunit inhibition is a direct modulation, i.e., after G-protein activation, $\beta\gamma$ subunits directly interact with VGCCs whereas phosphorylation of VGCCs requires activation of PKC, which in turns is the result of a long biochemical pathway (see schematic in Fig. 2).

From Section 4.1, the steady fraction of channels in the inhibited and phosphorylated state depends on $\eta = k_{\text{cat}}/\alpha_{\text{pkc}}$, the ratio between the PKC catalytic rate and the channel-dephosphorylation

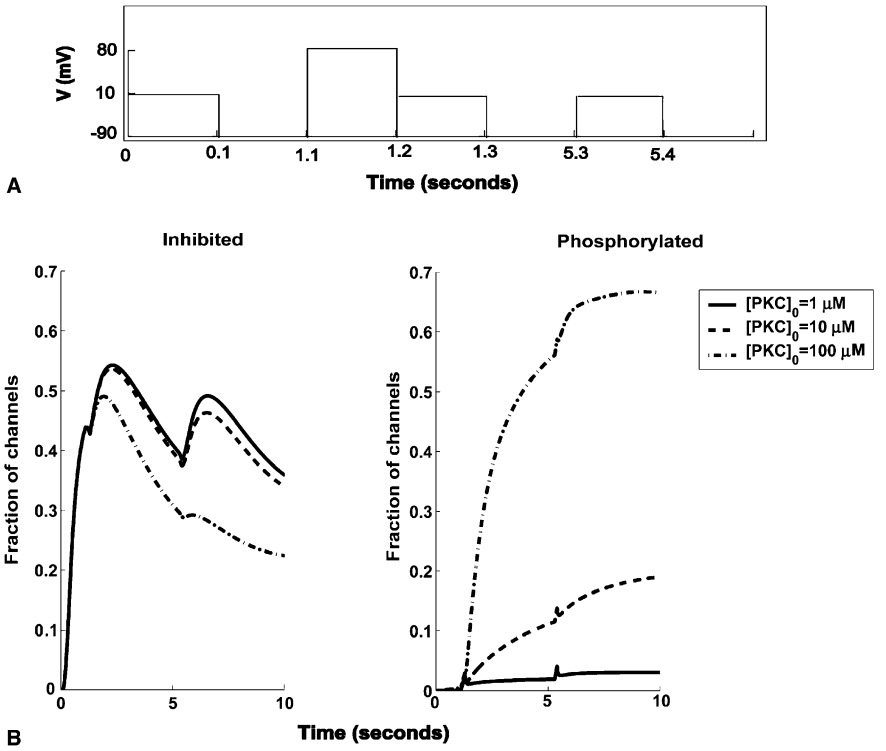

Fig. 6. Simulations of the full model. (A) Stimulation protocol used in [1]: 100 ms step depolarization to 10 mV initially, followed by 1 s at rest (−90 mV). Then there is a prepulse for 100 ms at 80 mV immediately followed by a 100 ms 10 mV depolarization. After 4 sec at rest (−90 mV) there is a third 100 ms depolarization at 10 mV, followed by return to the resting voltage. (B) The evolution of the fraction of channels in the inhibited (left panel) and phosphorylated (right panel) for different values of $[\mathrm{PKC}]_0$, under the stimulation protocol described before. Here we used high affinity autoreceptors, i.e., $K_{\mathrm{aut}} = 0.16\ \mu\mathrm{M}$ ($k_{m1} = 5\ \mathrm{s}^{-1}$), cf. Table 3.

rate. Because of the value of the calcium decay in the active zone, less than 1% of the total concentration of PKC is in the active state for time scales $\mathcal{O}(k_{\mathrm{act}}^{-1})$ (not shown). This implies that the dominant modulation is inhibitory on this time-scale. However, $\eta = \mathcal{O}(50)$, which indicates that a small increase in activated PKC concentration would lead to a large increase in the fraction of phosphorylated channels. Therefore, simulations showed that as the concentration of PKC increases at the terminal, $\beta\gamma$-subunit inhibition of VGCCs can be dramatically reduced, which could potentially affect vesicle release for long trains of stimulation ($\mathcal{O}(10)$ s).

After depolarization, the population of channels returns to steady state $[Wc] \sim 1$ i.e., all channels are in the closed, unmodulated state. The half-time before transition to another state from $R_{\mathrm{c}}^{\mathrm{Pr}}$, is given by $(\alpha'(V_{\mathrm{rest}}) + \alpha_p)^{-1}$, where $V_{\mathrm{rest}} \sim -90$ mV (cf. Fig. 4) i.e., the recovery rate depends on the relative size of α' and α_p. For the parameters used here, $\alpha'(V_{\mathrm{rest}}) \gg \alpha_p$, which implies that the probability of a channel switching from the R to the W state is much smaller that the probability of a channel in the R switching between the open and closed states. This suggests that neuronal activity induces a transient modulation (both inhibition and phosphorylation) whose decay

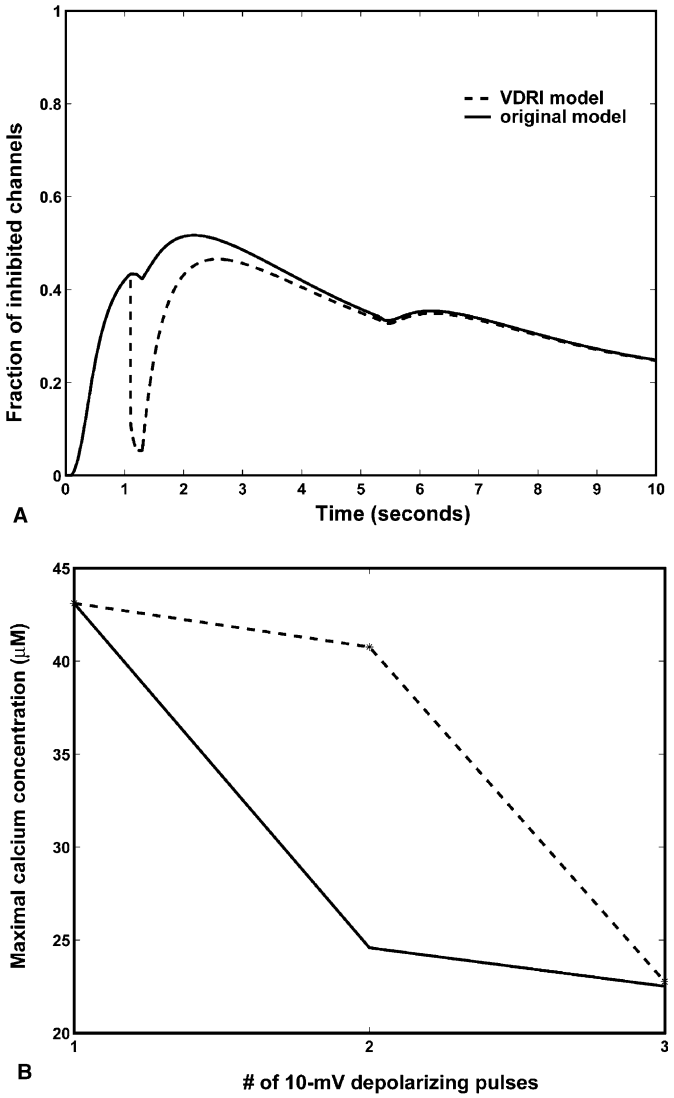

Fig. 7. A comparison of the evolution of the fraction of inhibited channels when we explicitly consider removal of $\beta\gamma$-subunit inhibition by strong depolarization. Panel A panel shows the evolution of inhibited channels with voltage-dependent release from inhibition (VDRI, solid lines), and without VDRI (original model, dashed lines). The 80 mV prepulse depolarization releases VGCCs channels from inhibition (approximately a 70% reduction of the fraction of inhibited channels after the prepulse in the VDRI model compared to the fraction of inhibited channels after the prepulse in the original model. Panel B: the maximal calcium concentration during the 10 mV depolarizations (see part A in Fig. 6, corresponding to the original model and the model with voltage-dependent release from inhibition. Here, $[\mathrm{PKC}]_0 = 1$ μM. The resting level of calcium is in the nanomolar range.

time depends on the kinetic parameters of the single channel dynamics. For the parameter choice, such slow decay can be correlated to the so-called tonic inhibition of N-type channels by $\beta\gamma$ subunits in [32].

Previous work in [8,33] suggested that release from inhibition of VGCCs by depolarization is significant for depolarizing voltages above 50 mV (in fact, experiments were only done with depolarizations between 100 and 150 mV [8,33]). Moreover, it was found that the release of inhibition by depolarization followed a sigmoidal-type relationship. To include this feature in our model, we can replace the constant parameter $\alpha_p = 0.25$ in (11), which corresponds to the rate for the transition from R_c^{Pr} to W_c, by $\alpha_p = 0.25 + 500(1 + \tanh(V - 50))$. (The voltage crossover was set at 50 mV to agree with the experimental findings and the multiplier set to obtain a significant effect on the rate.) We call this variation of the model the *voltage-dependent release from inhibition* (VDRI) model. Fig. 7 shows simulations of the original model and the VDRI model with the stimulation protocol as in Fig. 6(A). Panel A shows, as expected, that the 80 mV prepulse reduces the fraction of channels in the inhibited state from 40% to less than 10%. If we look at the maximal calcium concentration during each of the three 10 mV depolarization steps (Panel B in Fig. 7), we see that there is an 80% increase in calcium influx in the VDRI model, which is in qualitative agreement with the experimental results in Fig. 1 of [1]. During the third depolarizing pulse (Panel B in Fig. 7), the influx of calcium is the same in both models, which is also in agreement with experimental data in [1]. Note that the after the strong depolarization, the fraction of channels inhibited by $\beta\gamma$-subunits returns to levels similar to the ones in the original model on a time scale $\mathcal{O}(500)$ ms, which agrees with the measurements in [33].

Most plastic changes in the strength of synaptic connections are believed to occur after bursts of stimuli [25]. Since the activation of the modulatory mechanisms presented here occur on a slower time scale than the corresponding time scale for vesicle release, it is important to study how such mechanisms are affected by repeated stimulation. We ran simulations for the full model under different stimulation frequency and kinetic properties of autoreceptors to see how the strength of the modulation is affected. The stimulation protocol consists of periodic stimulation (repeated 1-ms step depolarizations from −90 mV to 10 mV) of the presynaptic terminal for one second under different frequencies. Fig. 8 shows, for different values kinetic properties of GPCRs, the peak fractions of inhibited and phosphorylated channels (parts A and B) as a function of the stimulation frequency. Part C of Fig. 8 shows how the maximal calcium concentration changes during the stimulation protocol as a function of the stimulation frequency, for different kinetic properties of GPCRs. As expected, the peak fraction of inhibited channels increases as the affinity of GPCRs increases (i.e., as K_{aut} decreases) (cf. Fig. 8(A)). Since $v = \mathcal{O}(1)$ ($k_{m1} = 5\ s^{-1}$), the peak fraction of inhibited channels is maximal when $K_{aut} = 0.16\ \mu M$, because the dynamics of GPCRs is dictated by $[N]/K_{aut}$. Since the decay time constant for neurotransmitter in the cleft is very rapid ($\mathcal{O}(10^6)\ s^{-1}$), N is very small on average during the stimulation. Note also that there is a saturation level for the peak fraction of inhibited channels which depends on the affinity of the autoreceptors.

Panel B of Fig. 8 shows the peak fraction of phosphorylated channels, and as in A for inhibited channels, the peak fraction of phosphorylated channels is the largest when K_{aut} is smallest. Moreover, note that as K_{aut} increases the curves shift to the right, which indicates that it becomes harder to obtain significant levels of phosphorylated channels as the affinity of the GPCRs decreases, even under repeated stimulation. Note also that for $K_{aut} = 0.16\ \mu M$, the peak fraction of phosphorylated channels remains roughly constant until the stimulation frequency surpasses approximately 40 Hz, which is $\mathcal{O}(k_{hyd})$, the decay time constant for α-subunits (G_α in the model). Beyond this frequency there is a net increase in G_α during the stimulation, which leads to an increase in the level of PKC^* and hence of the fraction of phosphorylated channels during stimulation.

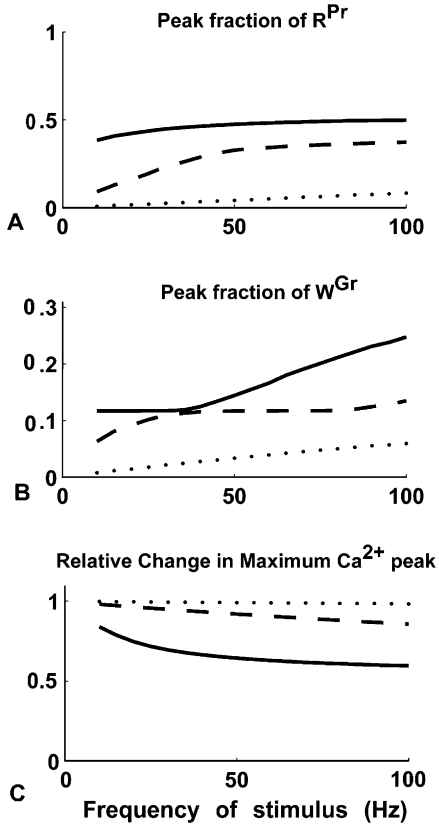

Fig. 8. Numerical simulations of the model when the terminal is periodically stimulated at different frequencies for 1 s (each action potential is modeled as a 1-ms 10 mV step depolarization). Panel A shows the peak fraction of inhibited channels for different values of the kinetic parameters of autoreceptors. Panel B shows the peak fraction of phosphorylated channels, and panel C shows the change in maximal calcium concentration between the first and last steps in the stimulation protocol. In all panels solid lines represent $K_D = 0.16$ μM, dashed lines represent $K_D = 1.6$ μM, and dotted lines represent $K_D = 16$ μM. In addition $k_{m1} = 5\ s^{-1}$ and $[PKC]_0 = 10$ μM in all panels.

Panel C in Fig. 8 shows how the maximal calcium concentration at the last depolarization step in the train of stimulation changes with respect to the maximal calcium concentration during the first depolarization step. In all cases, there is a reduction in the maximal calcium concentration which is due to the fact that the inhibitory pathway directly modulates VGGCs whereas the phosphorylation pathway is indirect. This is also reflected in Fig. 6, since after the first step depolarization, there is no change in the rate of increase of the fraction of inhibited channels, for different values of $[PKC]_0$.

To date, most experiments in which strong depolarizing stimuli were used to induce release from $\beta\gamma$-modulated inhibition of calcium channels found that stimulation times of the order of at least 30–40 ms were needed to induce significant release from inhibition; for instance in [33], 35-ms step depolarizations were applied at 0.25 Hz. If we repeat the simulations in Fig. 8 with the VDRI model, there would be no qualitative difference in the outcome. In fact, the time scale for release from inhibition by depolarization is of order 10 ms, for the parameters used here,

which is one order of magnitude larger that the time in which depolarization occurs. Even if we shift the voltage-threshold for the voltage-dependent release from inhibition in the VDRI model, the corresponding relationship between frequency and the peak fraction of either inhibited or phosphorylated channels obtained with the VDRI model will be still qualitatively the same as the ones presented in Fig. 8. This prediction could be tested experimentally.

6. Conclusions

We proposed a model for modulation of N-type channels located on the presynaptic face Γ_c based on the experimental findings in [1]. Our model consists of a feed-back loop involving neurotransmitters, VGCCs and autoreceptors. Perturbation analysis was used to uncover a hierarchy of times scales for such processes during neurotransmission. Our model reproduces the levels of $\beta\gamma$-modulated inhibition found experimentally in [1] (Fig. 6). The search for the many parameters involved in our model was extensive, since the different sub-processes involved in our proposed VGCC-regulation were studied in different experimental models, so we chose those parameters that gave simulation results similar to those observed experimentally.

Modulation of calcium influx through G_α-activation occurs on a slower time scale than the time scale in which transmitter release takes place, which suggests that under physiological conditions, only trains of action potentials would trigger such modulation. In particular, the kinetic properties of autoreceptors and the frequency of the stimuli would determine the dynamics of the proposed regulatory mechanism.

Under steady state levels of either $\beta\gamma$ subunits or activated PKC, the competitive nature of inhibition and phosphorylation depends on $\eta = k_{cat}/\alpha_{pkc}$. Since $\eta = \mathcal{O}(50)$ from Table 1, one can conclude that small increases in activated PKC would lead to a significant increase in the fraction of phosphorylated channels relative to the fraction of inhibited channels. As we decrease the value of η, by increasing the dephosphorylation rate α_{pkc}, the levels of phosphorylated channels decrease accordingly. In particular, when $\eta = \mathcal{O}(1)$ the maximal level of phosphorylated channels strongly depends on the rate at which calcium decays in the active zone. In particular, when buffer species are present in the cytoplasm, the kinetic properties of buffers determine how fast calcium returns to basal levels, hence it will modulate the levels of activated PKC [30].

The parameter $\nu = k_{m1}/k_{act}$ (the ratio between the unbinding rate between autoreceptors and neurotransmitters and the G-protein activation rate) allows us to determine, depending on the kinetic properties of the autoreceptors, how this modulatory process depends on the frequency of the stimulation. For $\nu \gg 1$, the assumption that neurotransmitters and autoreceptors are in pseudo-equilibrium holds. However, in physiological conditions, $N \ll 1$ on the time scale $\mathcal{O}(k_{act}^{-1})$ (clearance of neurotransmitters in the cleft is faster than k_{act}^{-1} [26], which implies that only high affinity receptors ($K_{aut} \ll 1$) would trigger VGCC-modulation. If $\nu = \mathcal{O}(1)$, then neurotransmitters and autoreceptors are no longer in pseudo-equilibrium. In particular, K_{aut} determines a threshold value for stimulation frequency such that above this threshold, VGCC regulation would be tonic (cf. Fig. 8), and depending on whether $\beta\gamma$ inhibition of PKC phosphorylation are the dominant modulatory mechanism, it is possible to induce up- or down-regulation of transmitter release, by increasing stimulus frequency.

The simulations (cf. Fig. 6) suggest that down-regulation of VGCCs by $\beta\gamma$ subunits will prevail for concentrations of PKC of order 10 μM under one or a few depolarizing stimuli. This is a consequence of the fact that VGCC regulation by PKC follows an indirect biochemical pathway (cf. Fig. 2), whereas $\beta\gamma$ modulation consists of a single kinetic step after G-protein activation. This also depends on the fact that calcium decay in the active zone is faster than k_{hyd}^{-1}, the rate of GTP-hydrolysis (cf. Eq. (39)). In particular, the intracellular calcium increases on the slower time scale are not sufficient to elicit a substantial increase in activated PKC levels so that it can compete with $\beta\gamma$ subunits. But, DAG-generation occurs on a time scale $\mathcal{O}(k_{\text{hyd}}^{-1})$ greater than the G-protein activation time scale (hence $\beta\gamma$ modulation), which implies that if significant increases in calcium concentration are sustained on the time scale for DAG-activation, PKC-modulation would prevail over $\beta\gamma$ subunit down-regulation. Regulation of the intracellular calcium increases depend on processes such as buffering, and depending on the kinetic properties of the species, it is possible to obtain either up- or down-regulation of VGCCs according to the buffer species present in the presynaptic terminal [30].

However, the model also suggests a self-regulatory mechanism for transmitter release under repeated stimulation. We predict that sustained activity leads to down-regulation of VGCCs, which results in a decrease in the maximal calcium concentration at the terminal, which in turn effectively decreases the probability of vesicle release (Figs. 6–8). Nonetheless, the synapse can recover from inhibition by phosphorylation of VGCCs i.e., increase of fraction of phosphorylated channels, on a time scale determined by the levels of PKC (Fig. 6) and the decay time constant for calcium (data not shown, see [30]. This in turn would increase the calcium influx and thereby increase the probability of vesicle release.

A prediction of our model is that for suitable kinetic properties of GPCRs, there is a particular frequency at which the peak fraction of phosphorylated channels changes: in our model is 40 Hz, i.e., k_{hyd}^{-1} (cf. Fig. 8). Below that frequency the peak fraction of phosphorylated channels remains constant. Above that frequency, there is a monotonic increase in the peak fraction of phosphorylated channels as the frequency of the stimulus increases (solid line in Fig. 8). This implies that there would be a decrease in the levels of $\beta\gamma$-subunit inhibition of VGCCs as the frequency of stimulation increases. If we were to deliver a stimulus at the time in which the peak fraction of modulated channels occurs (the maximal fraction of either phosphorylated or inhibited channels occur around 7–10 s, data not shown), this will lead to an increase in the calcium influx if the previous stimulation frequency was higher than 40 Hz, whereas if the previous stimulus frequency was less than 40 Hz, there would be no apparent change in the influx of calcium. This would be also true if instead of calcium influx, we were measuring neurotransmitter release. In particular, by changing the speed of hydrolysis of GTP (k_{hyd}), one should be able to change the frequency at which there is a change in the influx of calcium or neurotransmitter release.

It is known that strong depolarizations induce a release from $\beta\gamma$ inhibition in N-type calcium channels [32]. When we impose strong depolarizations in our model (80 mV step depolarizations) we only observe a small reduction in the fraction of inhibited channels, which is not in qualitative agreement with experimental data [8,33,1]. If we add to our model a voltage-dependent release from inhibition (Fig. 7), we are able to qualitatively match the effects of strong depolarizing prepulses on the short time scale (i.e., the reduction in the fraction of channels in the inhibited state) and we also showed that the results qualitatively matched the recovery time scale for the inhibition of VGGCs by $\beta\gamma$-subunits. In light of the time scales for the onset and recovery of VDIR, we

can assert that the simulation results in Fig. 8, i.e., the relationship between peak fraction of modulated channels and the frequency of stimulation, would not be altered if we explicitly consider a VDIR mechanism. A more detailed model for the voltage dependence of VGCCs, as in [14], would be needed when addressing how the presence of autoreceptors affects the local excitability properties of the cell membrane, for instance activation of calcium-dependent potassium and GIRK currents [34], or whether activation of autoreceptors would lead to better synchronization properties of neurons in the olfactory bulb [35], which in turn would have an effect on synaptic transmission. Coupling this biochemical model with a Hodgkin–Huxley type model for generation of action potentials would give us a way to address the effect of biochemical vs. electrical modulation of calcium influx [36]. There is a large body of experimental evidence that autoreceptors inhibit vesicle release. On the other hand, recent experiments suggest that autoreceptor activation induces an increase in vesicle release [13]. We propose an alternative mechanism for modulation of vesicle release via regulation of calcium influx through VGCCs. One of the predictions from the analysis of the model was that $\eta = k_{\mathrm{cat}}/\alpha_{\mathrm{pkc}}$ determines the strength of the competition between inhibition and phosphorylation. For systems in which vesicle release is mainly regulated by N-type channels, it would be interesting to see whether changes in the channel dephosphorylation rate would lead to changes in the levels of inhibition and phosphorylation of calcium channels in the presynaptic terminal. In this way, it would be possible to elucidate whether small or large increases in activated PKC are needed to remove $\beta\gamma$-inhibition under repeated stimulation. The generation of activated PKC was based upon a simplified kinetic scheme. However, more detailed molecular mechanisms for PLC-generation, PIP_2 cleavage and PKC generation are now available, and one can obtain a more realistic scheme for the regulation of VGCCs via downstream effectors of G-protein activation.

Acknowledgments

We like to thank Jon Gottesman for the useful discussions and inputs to this work. This work has been supported by NIH grant 29123 and by the Facultad de Ingeniería of Universidad Nacional de la Patagonia San Juan Bosco.

References

[1] C.F. Barrett, A.R. Rittenhouse, Modulation of N-type calcium channel activity by G-proteins and protein kinase C, J. Gen. Physiol. 115 (3) (2000) 277.
[2] B. Katz, The Release of Neural Transmitter Substances, Liverpool University, Liverpool, United Kingdom, 1969.
[3] C.J. Meinrenken, J.G. Borst, B. Sakmann, Local routes revisited: the space and time dependence of the Ca^{2+}signal for phasic transmitter release at the rat calyx of held, J. Physiol. 547 (Pt 3) (2003) 665.
[4] M.J. Berridge, The endoplasmic reticulum: a multifunctional signaling organelle, Cell Calcium 32 (5–6) (2002) 235.
[5] T.C. Sudhof, The synaptic vesicle cycle, Annu. Rev. Neurosci. 27 (2004).
[6] W.A. Catterall, Structure and function of neuronal Ca^{2+} channels and their role in neurotransmitter release, Cell Calcium 24 (5–6) (1998) 307.
[7] B. Hille, Ionic Channels of Excitable Membranes, Sinauer Associates Inc., Sunderland, Massachussets, 1992.

[8] L.M. Boland, B.P. Bean, Modulation of N-type calcium channels in bullfrog sympathetic neurons by luteinizing hormone-releasing hormone: kinetics and voltage dependence, J. Neurosci. 13 (2) (1993) 516.
[9] K.J. Swartz, Modulation of Ca^{2+} channels by protein kinase C in rat central and peripheral neurons: disruption of G-protein-mediated inhibition, Neuron 11 (2) (1993) 305.
[10] M.R. Bennett, The concept of a calcium sensor in transmitter release, Prog. Neurobiol. 59 (3) (1999) 243.
[11] K. Starke, Presynaptic autoreceptors in the third decade: focus on α^2-adrenoceptors, J. Neurochem. 78 (4) (2001) 685.
[12] T. Yoshitake, S. Yoshitake, M. Yamaguchi, S.O. Ogren, J. Kehr, Activation of 5-HT(1A) autoreceptors enhances the inhibitory effect of galanin on hippocampal 5-HT release in vivo, Neuropharmacology 44 (2) (2003) 206.
[13] H. Vitten, J.S. Isaacson, Synaptic transmission: exciting times for presynaptic receptors, Curr. Biol. 11 (17) (2001) R695.
[14] R. Bertram, M. Behan, Implications of G-protein-mediated Ca^{2+} channel inhibition for neurotransmitter release and facilitation, J. Comput. Neurosci. 7 (3) (1999) 197.
[15] R. Schneggenburger, E. Neher, Intracellular calcium dependence of transmitter release rates at a fast central synapse, Nature 406 (6798) (2000) 889.
[16] A.M. Thomson, Facilitation, augmentation and potentiation at central synapses, Trends Neurosci. 23 (7) (2000) 305.
[17] S. Weis, R. Schneggenburger, E. Neher, Properties of a model of Ca^{2+}-dependent vesicle pool dynamics and short term synaptic depression, Biophys. J. 77 (5) (1999) 2418.
[18] J.S. Dittman, A.C. Kreitzer, W.G. Regehr, Interplay between facilitation, depression, and residual calcium at three presynaptic terminals, J. Neurosci. 20 (4) (2000) 1374.
[19] Y. Tang, H.G. Othmer, Excitation, oscillations and wave propagation in a G-protein-based model of signal transduction in *dictyostelium discoideum*, Philos. Trans. R. Soc. Lond. B: Biol. Sci. 349 (1328) (1995) 179.
[20] J. Zhou, M.S. Shapiro, B. Hille, Speed of Ca^{2+} channel modulation by neurotransmitters in rat sympathetic neurons, J. Neurophysiol. 77 (4) (1997) 2040.
[21] S. Mukhopadhyay, E.M. Ross, Rapid GTP binding and hydrolysis by G(q) promoted by receptor and GTPase-activating proteins, Proc. Natl. Acad. Sci. USA 96 (17) (1999) 9539.
[22] T. Meyer, D. Holowka, L. Stryer, Highly cooperative opening of calcium channels by inositol 1,4,5-trisphosphate, Science 240 (4852) (1988) 653.
[23] S.G. Rhee, Regulation of phosphoinositide-specific phospholipase C, Annu. Rev. Biochem. 70 (2001) 281.
[24] K.H. Yang, J.H. Kotaleski, K.T. Blackwell, The role of protein kinase C in the biochemical pathways of classical conditioning, Neurocomputing (2001) 79.
[25] M.J. Zigmond, F.E. Bloom, S.C. Landis, J.L. Roberts, L.R. Squire, Fundamental Neuroscience, Academic Press, 1999.
[26] D.E. Bergles, J.S. Diamond, C.E. Jahr, Clearance of glutamate inside the synapse and beyond, Curr. Opin. Neurobiol. 9 (3) (1999) 293.
[27] R.S. Zucker, Exocytosis: a molecular and physiological perspective, Neuron 17 (6) (1996) 1049.
[28] E.A. Fon, R.H. Edwards, Molecular mechanisms of neurotransmitter release, Muscle Nerve 24 (5) (2001) 581.
[29] G.D. Smith, L. Dai, R.M. Miura, A. Sherman, Asymptotic analysis of buffered calcium diffusion near a point source, SIAM J. Appl. Math. 61 (5) (2001) 1816.
[30] G.R. Soto, An integrated model for calcium dynamics during synoptic transmission, Ph.D. thesis, University of Minnesota, 2003.
[31] J.G. Borst, B. Sakmann, Calcium influx and transmitter release in a fast CNS synapse, Nature 383 (6599) (1996) 431.
[32] A.C. Dolphin, Mechanisms of modulation of voltage-dependent calcium channels by G-proteins, J. Physiol. 506 (Pt 1) (1998) 3.
[33] A. Golard, S.A. Siegelbaum, Kinetic basis for the voltage-dependent inhibition of N-type calcium current by somato-statin and norepinephrine in chick sympathetic neurons, J. Neurosci. 13 (9) (1993) 3884.
[34] C. Koch, Biophysics of Computation: Information Processing in Single Neurons, Oxford, 1999.
[35] N.E. Schoppa, G.L. Westbrook, AMPA autoreceptors drive correlated spiking in olfactory bulb glomeruli, Nat. Neurosci. 5 (11) (2002) 1194.

[36] R. Bertram, M.I. Arnot, G.W. Zamponi, Role for G-protein $G_{\beta\gamma}$ isoform specificity in synaptic signal processing: a computational study, J. Neurophysiol. 87 (5) (2002) 2612.
[37] A.C. Newton, Regulation of protein kinase C, Curr. Opin. Cell Biol. 9 (2) (1997) 161.
[38] E. Oancea, T. Meyer, Protein kinase C as a molecular machine for decoding calcium and diacylglycerol signals, Cell 95 (3) (1998) 307.